Optimizing the Shape of SiO2 Anti-Reflective Microstructures on the Cover Glass of a Solar Panel

Aakash Joshi

Abstract

Developing a more efficient solar panel is an essential task to accelerate the deployment of solar photovoltaics to solve the world's energy crisis. A common way to maximize energy output is to reduce the amount of sunlight reflected off the solar panel via geometric anti-reflection coatings (ARCs). These microstructures prevent light from escaping the solar panel. Utilizing the ray-tracing software, pvtrace, the shape and dimensions of these microstructures were optimized to maximize the amount of light that passes through to the solar cell. The shapes simulated were pyramids, cylinders, cones, and mounds of the material silicon dioxide (SiO_2), a common ARC material. For normal angles, the optimized pyramid texture had the greatest light transmission of 0.93. This geometric ARC texture would be most relevant for solar panels with dual-axis tracking that can ensure sunlight approaches the panel at a normal angle. At non-normal incidence angles, different geometries were optimal, with no clear geometry outperforming others at all angles. However, taking an average weighted by solar insolation and the daily solar cycle (relevant to fixed solar panels), the most optimal geometry is a mound structure that produces an average transmission of 0.90. This research identified the most optimal shape and dimension to consider when developing geometric ARCs to maximize light transmission for fixed and dual-axis tracking solar panels, allowing expansion of solar power generation capabilities.

Introduction

Combating climate change and fossil fuel dependency will require the use of renewable energy sources, like solar power. There are many techniques to optimize the efficiency of solar cells to increase energy output; a prominent one is antireflection coatings (ARCs), which enhance the amount of light available for photovoltaic (PV) conversion, improving solar cell performance [1]. The ARCs raise the level of light absorption by minimizing the amount of light reflected. Particularly, this can be accomplished at the air/glass substrate interface [2].

This research focuses specifically on geometric ARCs, which enhance performance by increasing the number of times light bounces [2]. As seen in Figure 1, increasing the number of bounces with some sort of angled surface creates more opportunities for light to pass through. The main advantage of geometric ARCs is that they work for all wavelengths of light, preserving spectral independence, provided that the features of the textured geometric ARC are much larger than the wavelengths of interest [2]. Thus, while both microstructures and nanostructures have been proposed, microstructures are of interest to maintain the anti-reflective effect for light in the visible and infrared light range [2], [3].

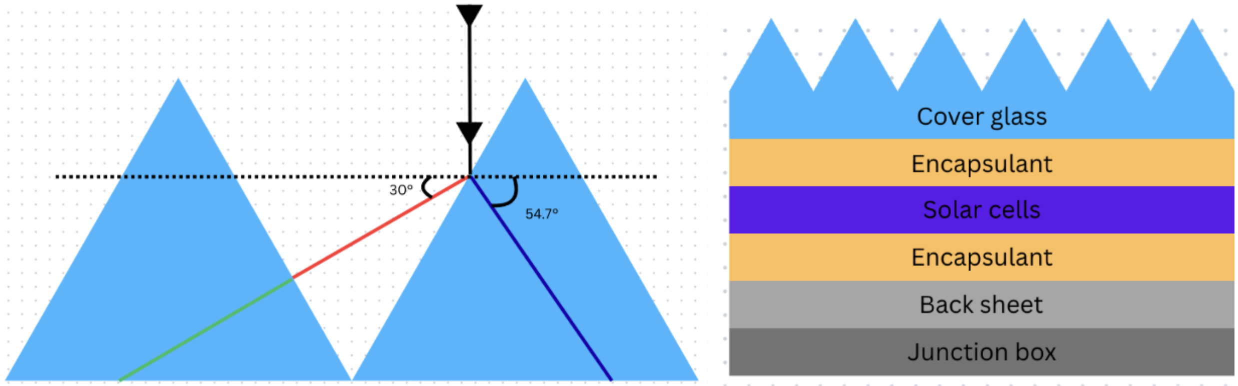

Figure 1: The left side shows how an ARC texture with a refractive index of 1.5 promotes the transmittance of both refracted and reflected light. The right side shows the geometric ARCs' location.

Implementation of geometric ARCs can be done at different layers within a solar panel. Light-trapping microstructures and nanostructures could be embedded within the absorber layer of solar cells. However, microstructures can be impractical at the absorber layer for thin-film solar cells, as micron-scale features would be difficult to incorporate on a thin substrate [4]. In contrast, due to the thicker cover glass and encapsulant layers, either microstructures or nanostructures can be used here. Some research has been done on textured patterns placed on the cover glass of thin-film solar panels as well, marking significant increases in conversion efficiency and photocurrent, although the amount of research is minimal [5]. Countless materials, such as magnesium fluoride (MgF2), titanium dioxide (TiO2), zirconium dioxide (ZrO2), zinc oxide (ZnO2), aluminum oxide (Al2O3), and polymethyl methacrylate (PMMA), paired with countless geometries like rods, pyramids, pillars, cones, and tips, have been tested for ARCs with placement surrounding the cover glass in prior research [1], [6]. Several of these materials have self-cleaning and other unique properties [6]. Embedding these structures in the cover glass of solar panels in outer space has also been studied [7]. Physical development and experimentation of the textured patterns were conducted previously, marking increases in photocurrent and power, but identification of the optimal shape and dimensions has not been extensively explored. The process of ray-tracing can prove to be advantageous since computing the full electromagnetic wave calculation could be expensive and time-consuming, whereas ray-tracing is much faster and still has practical relevance for micron-scale features. Namely, if the texturization period, or the gap between the individual structures of the geometric ARCs, is much longer than the wavelength of light being analyzed, ray-tracing methods are suitable to determine optical properties [8]. This study uses ray-tracing simulations to optimize the shape and dimensions of microstructures placed on the cover glass of the solar cell along the air/glass interface to maximize light absorption.

Methods

a) Materials and Processes

To simulate the movement of light rays, a ray-tracing method was employed. In ray-tracing, light rays are initialized at different locations above a designated surface at a specific angle, and their path traversals are modeled. For example, a singular light ray that hits a boundary between two mediums may be reflected or refracted through the object based on its wavelength and the refractive indices and geometries of the involved objects and mediums. Ray-tracing is a technique to model many of these rays at once to observe the overall transmission and reflection proportions of the designated surface.

There are specific parametric inputs required for simulation: the number of light rays, the range of light wavelengths, the waveguide background absorption number (parasitic absorption), and the refractive index of the designated surface. An assumption that any light that is transmitted is absorbed by the solar cell was made as well.

The material of the geometric ARCs that was selected for this simulation was SiO2, a common material for anti-reflective coatings in prior implementations and experiments. Advantages of SiO2 are speedy production methods, relatively low costs, and great precision [9]. Mainly, the cover glass itself is typically either completely SiO2 or a composite in which the majority compound is SiO2, so integrating the geometric ARC textures into the cover glass would be simplified. Moreover, the results of the ray-tracing simulations for all geometries would apply to all types of solar cells, as no modifications were conducted to the solar cell itself.

b) Simulation Process

The simulation software used for the ray-tracing was pvtrace [10], [11], [12]. 10,000 light rays were simulated from a wavelength range of 300nm to 900nm. These wavelengths were chosen because they are between the start of the solar spectrum and the maximum wavelength at which a silicon solar cell would absorb light. The waveguide background absorption number, or the parasitic absorption, was set to 0, as at such small scales, it is negligible - SiO2’s absorption coefficient is minuscule, especially in the visible range, around $10^{-5}cm^{-1}$ at a wavelength of 1 micron [13]. The refractive index was set to be 1.5, which is approximately equivalent to the true refractive index of SiO2, ranging from 1.55 to 1.4 in its transparent range of 160nm to 3000nm [13], [14], [15].

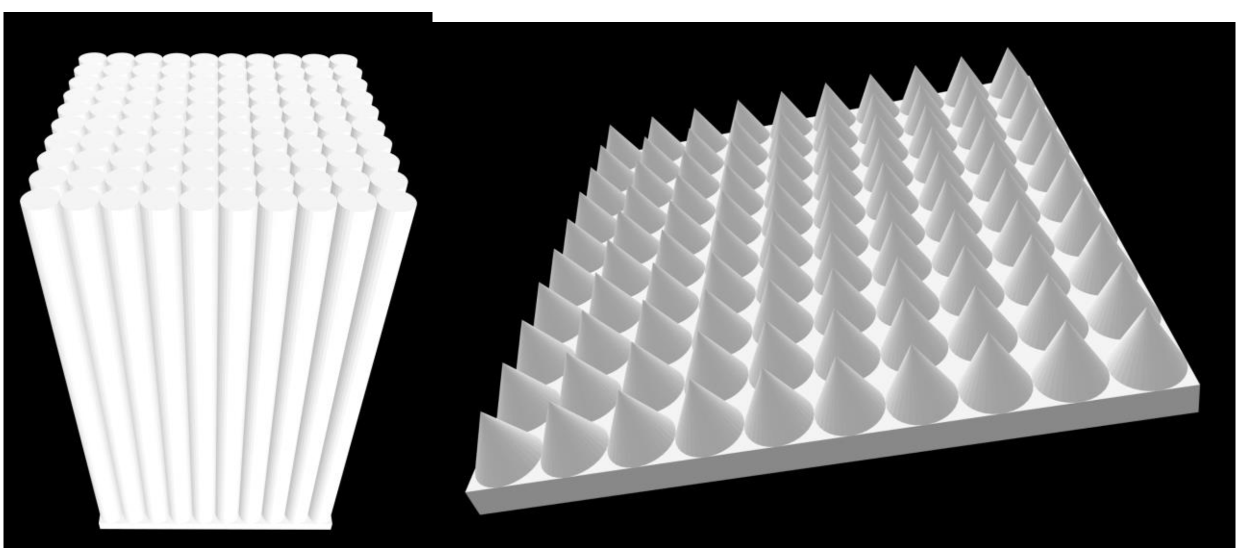

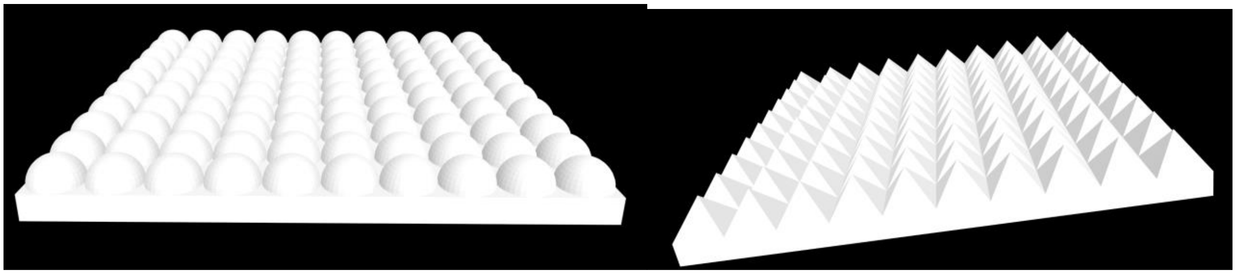

Figure 2: The 4 types of structures that were created using Autodesk Fusion CAD are cylinders, cones, mounds, and pyramids.

A 10 by 10 grid of individual, identical geometric ARC structures was developed on a square base, as shown in Figure 2. The structures are packed together, meaning that adjacent cylinders, cones, and mounds touch each other at one point on the base, whereas adjacent pyramids share a side at the base. The base, which was consistently kept the same size throughout the simulations, has dimensions of 1 unit x 1 unit x 0.05 units. Each texturization ARC pattern contained exactly 100 structures, as each structure's width was set to 0.1 units, allowing a 10x10 grid to be created on the base. The scale of the CAD files is inconsequential, as the ray-tracing simulation is agnostic of units and depends only on ratios, relative lengths, and sizes to track ray movement. In real applications, we envision the scale of the ARCs to be tens of microns. Also, the base, which appears in the following results as an aspect ratio (height divided by diameter or side length) of 0, served as a control group. The heights of the shapes were scaled and simulated until a clear, identifiable, optimal shape was discovered with a wide range of heights. The results were recorded.

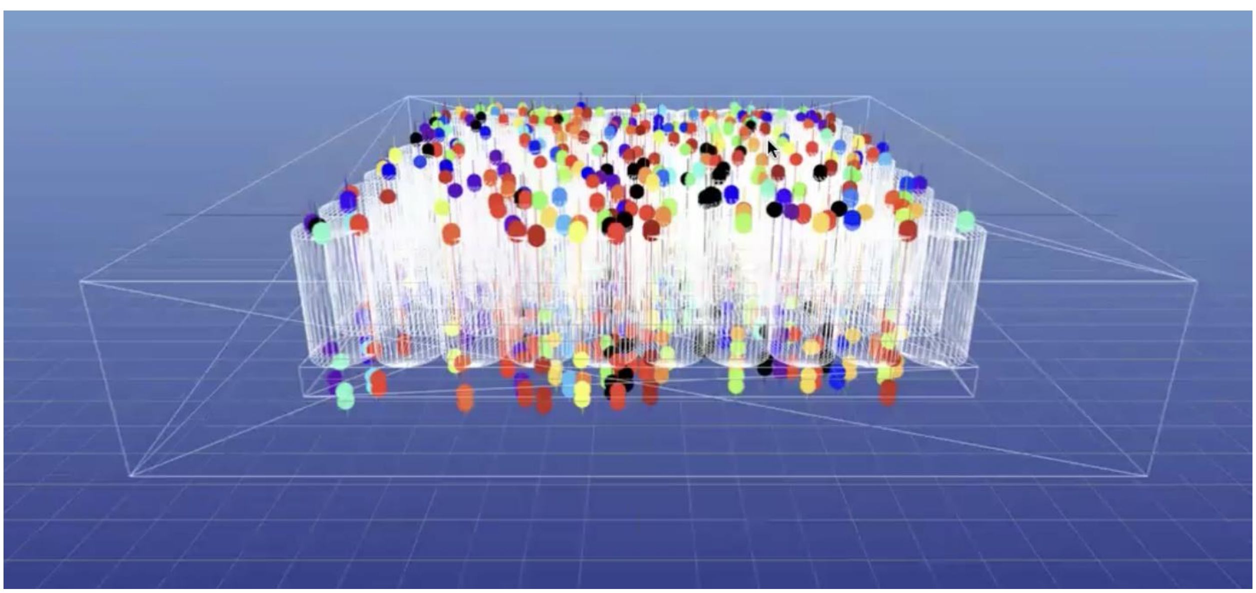

Figure 3: This is an example image of a ray-tracing simulation of a cylinder geometric ARC.

During the simulations, an enclosing box (shown in Figure 3) was included to allow simpler identification of the position of individual rays when exiting the structure. This would also enable the implementation of periodic boundary conditions, where rays that exit from the edge of the solar cell are passed on to another identical set of geometric ARCs until the ray exits from the top or bottom of the solar panel due to refraction, mimicking macro-scale solar panels. Implementing periodic boundary conditions is a potential case for future research. By selecting to maximize transmission, all of the light emitted from the edges of the structure, which would typically be passed on to additional geometric ARCs, is assumed to be reflected. Because this worst-case scenario is held to be true, it is logical to maximize transmission rather than solely minimize top reflection, as minimizing top reflection would ignore the proportion of edge emission light that is reflected, resulting in an inadequate optimization.

Additionally, the transmission, defined as the proportion of rays that exit the structure from the bottom, was the main performance metric. For light rays with a non-zero angle of incidence, the simulation halts either once all 10,000 light rays are traced or once the simulation results converge. When the difference between the current transmission (which includes the current ray being simulated) and the transmission of all other simulated rays (meaning that adding a new ray does not change this transmission) is less than the convergence threshold of $1x10^{-5}$, the simulation converges and stops running. This convergence process speeds up simulation times. On a laptop with 8GB of RAM and an Apple M2 processing chip, some of the mound structures can take roughly 30 minutes to simulate, compared to the other structures, which only took a few minutes, likely due to the many triangular surfaces needed to replicate the hemispherical geometry in a mesh file.

Results and Discussion

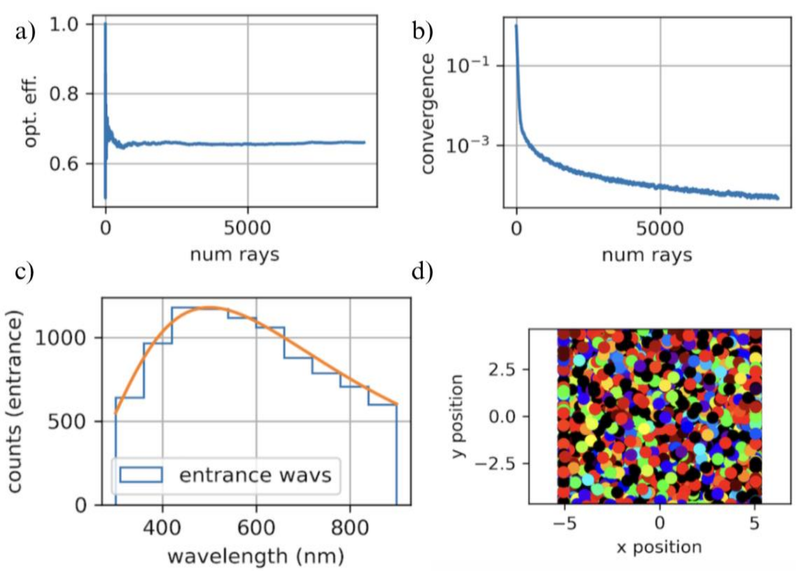

Figure 4: This is an example of the results produced by the software for a cone texture with light rays at an angle of incidence of 30° for a simulation that converged slightly before 10,000 rays.

For each geometry and angle considered, the transmission properties and the simulation information were recorded, as shown in Figure 4. The transmission, noted as optical efficiency in Figure 4(a), reaches a value between 0.6 and 0.8. Figure 4(b) shows that the simulation reaches the threshold of $1x10^{-5}$, converging shortly before tracing all

10,000 rays. Figure 4(c) shows a histogram of the frequency of initiated rays that fall into each wavelength interval, closely resembling visible light’s intensity properties. Figure 4(d) simply shows the position of the light rays.

Next, plots of transmission versus aspect ratio were created for every geometry’s performance for each incident angle. The left-hand side contains the entire dataset, whereas the right-hand side contains a zoomed-in version of the graph in the optimal transmission region.

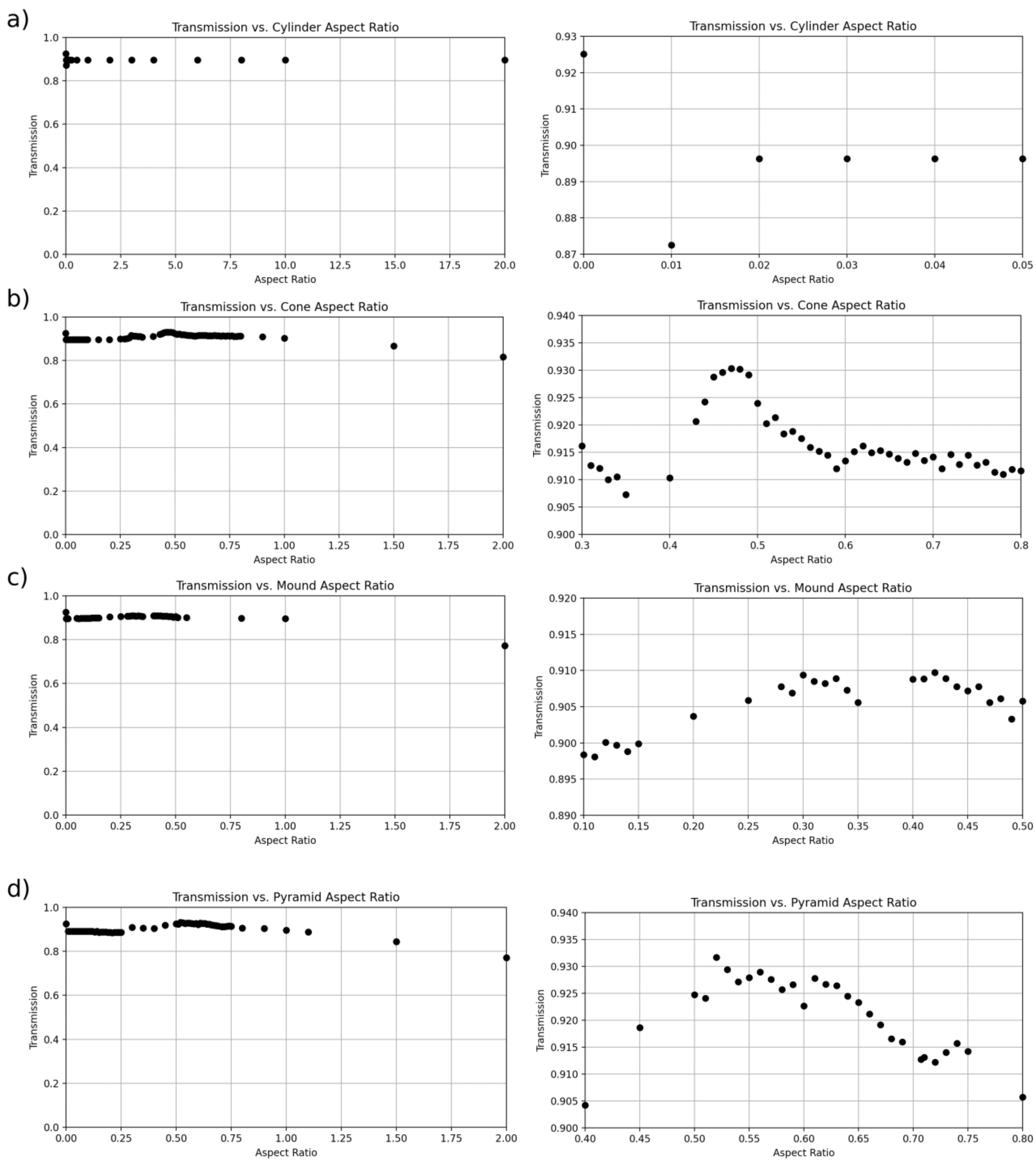

Figure 5: The graphs plot the data recorded for light rays normal to the surface (incident angle of 0°) for each geometry, with a zoom-in on the region containing the optimal transmission range.

For light rays normal to the surface, the best-performing geometry was a pyramid pattern found at point (0.52, 0.9317) in Figure 5(d). This was the highest transmission recorded throughout the experiment as well. The point (0, 0.9251) in Figure 5(a) and Figure 5(c), which is the maximum in these plots, demonstrates how a flat base serving as the control outperforms mound and cylinder geometries for incident angles of 0°.

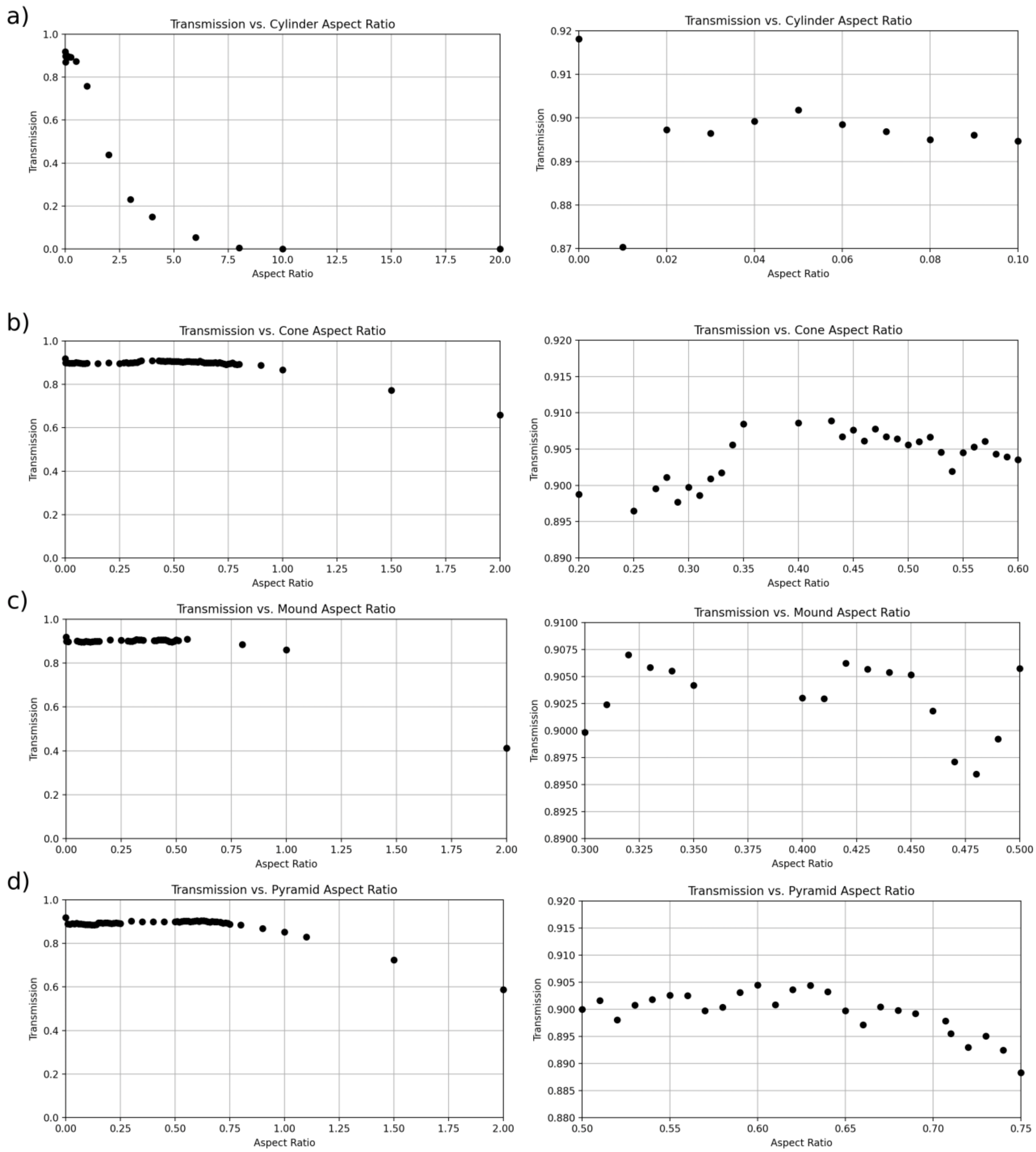

Figure 6: The graphs plot the data recorded for light rays initiated at an incident angle of 30° for each geometry, with a zoom-in on the region containing the optimal transmission range.

For an angle of incidence of 30°, as shown in all of Figure 6, each of the 4 geometries was outperformed by the flat control group, which is shown on the plots as point (0, 0.9181). The next best-performing geometry was the cone texture at point (0.43, 0.9089) in Figure 6(b).

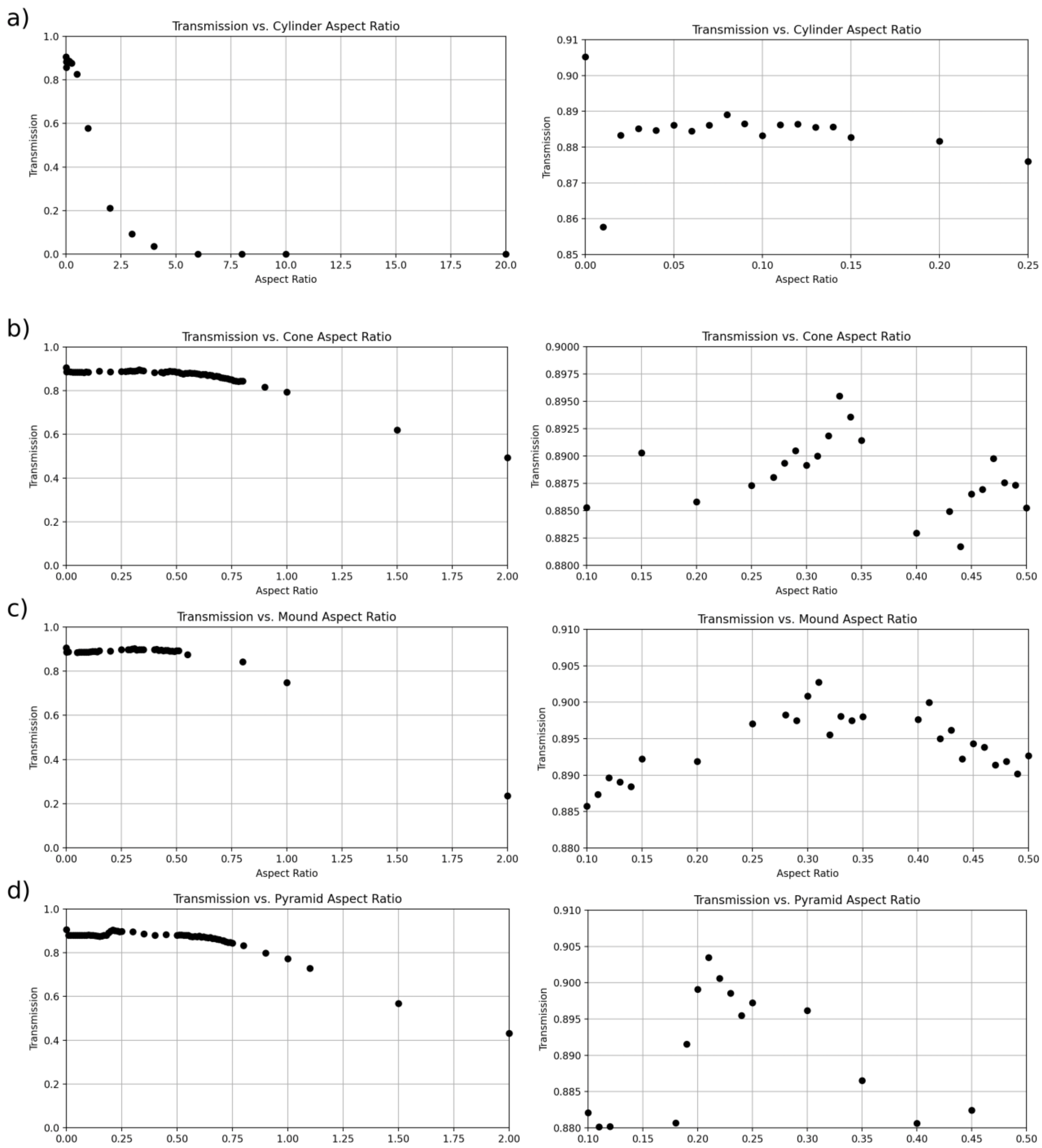

Figure 7: The graphs plot the data recorded for light rays initiated at an incident angle of 45° for each geometry, with a zoom-in on the region containing the optimal transmission range.

For an angle of incidence of 45°, as shown in all of Figure 7, each of the 4 geometries was outperformed by the flat control group, which is shown on the plots as point (0, 0.9052). The next best-performing geometry was the pyramid texture at point (0.21, 0.9035) in Figure 7(d).

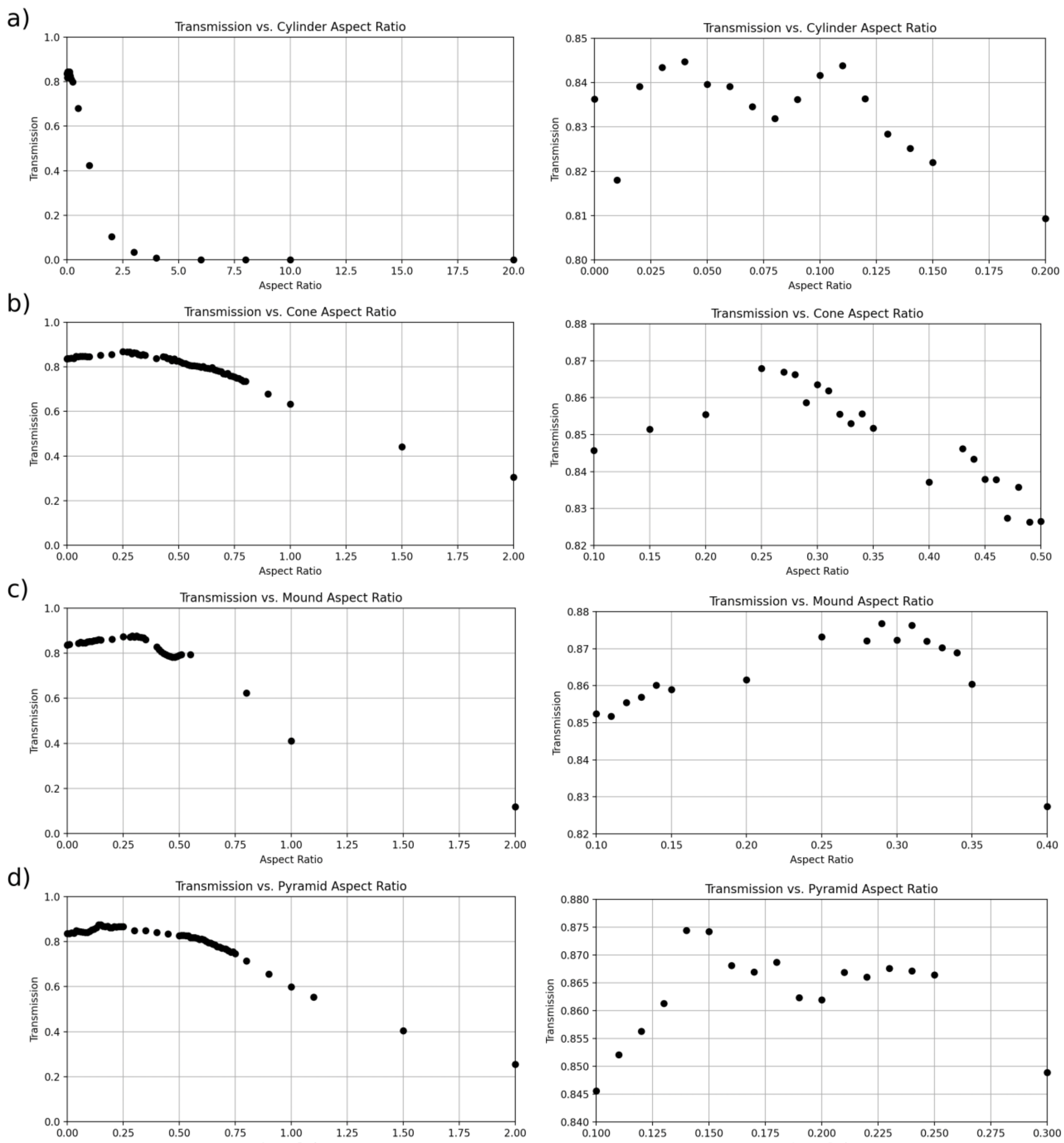

Figure 8: The graphs plot the data recorded for light rays initiated at an incident angle of 60° for each geometry, with a zoom-in on the region containing the optimal transmission range.

For an angle of incidence of 60°, as shown in Figure 8, the flat control group recorded an alarmingly low transmission of 0.8362. Each of the 4 geometries had aspect ratios that exceeded the flat control group's transmission. The best-performing geometry was a mound pattern seen as the point (0.29, 0.8768) in Figure 8(c).

Overall, the cylinders had the poorest-performing geometric ARC pattern, consistently failing to attain a transmission of 0.9 or higher across all but one incident angle. This may be due to the fact that the cylinder texture has vertical sidewalls, promoting outward light reflection rather than internal light redirection. Notably, the cylinder texture's transmission began to dramatically reduce as the height-to-diameter ratio increased for non-zero incident angles. For light normal to the surface, having an incidence angle of 0°, the cylinder texture maintained a nearly constant transmission no matter the height. Once parasitic absorption is considered, a greater drop-off in transmission should be expected with increasing cylinder height.

All structures performed worse at greater incident angles, which is in conformance with previous research that has found that an increase in angle of incidence corresponded to a reduction in transmittance [16]. Additionally, as the incident angle increased, the best-performing mound-shaped geometry experienced a lesser relative transmission decrease in comparison to the other geometries, such as cones and pyramids, which experienced a greater fall in transmission. This may be because of the steep surfaces of cones and pyramids that reflect light away at larger incident angles, contrasting with the smooth, gentle curvature of mounds. These results indicate that mound structures are the most resistant geometry to incident angle fluctuations.

As the incident angle increased, the most optimal cone geometry began to occur at smaller aspect ratios, meaning the geometry had shallower slopes. Interestingly, the mound and pyramid geometries followed a similar pattern, although this trend was not as consistent as it was for cones. As the incident angle increased, the maximum light transmission began to occur at smaller aspect ratios for all three geometries. However, this trend failed to apply to the cylinder geometry, which did not appear to have any discernible trend in aspect ratio in relation to incidence angle.

In summary, for normal incidence, the pyramid structure with a height-to-side ratio of 0.52 was the best-performing, producing a transmission of 0.93. This aligns with previous research, which found that the pyramid texturization was found to be the most optimal for nanostructures at a differing solar cell anatomical location [17]. This superior performance can be attributed to the geometrical quality of sloped surfaces, which redirect light deeper into the ARC and solar panel, as previously demonstrated in Figure 1. For both 30° and 45°, the flat control produced the greatest transmission of 0.92 and 0.91, respectively. Finally, for 60°, the mound geometry with a height-to-diameter ratio of 0.29 produced the greatest transmission of 0.88.

To generalize results across different incident angles in order to find the true optimal geometry, some sort of calculation regarding the sun's intensity at specific times and time spent at certain incident angles needed to be computed. Solar insolation and angle of incidence at every hour of active solar time were obtained from reference [18]. Then, to perform a weighted average of transmission across incident angles, the angles were assigned weights equivalent to the solar insolation at that angle's hour mark divided by the sum of the solar insolation values across the active solar times presented. Next, to predict a geometry's transmission for the data's given incident angles from reference [18], a quartic regression model (y axis - transmission, x axis - incident angle) built off the simulation data was created for each individual geometry. Finally, a weighted average transmission value was calculated by multiplying the weights by the predicted transmission at the given incident angle and summing these values up for a specific geometry.

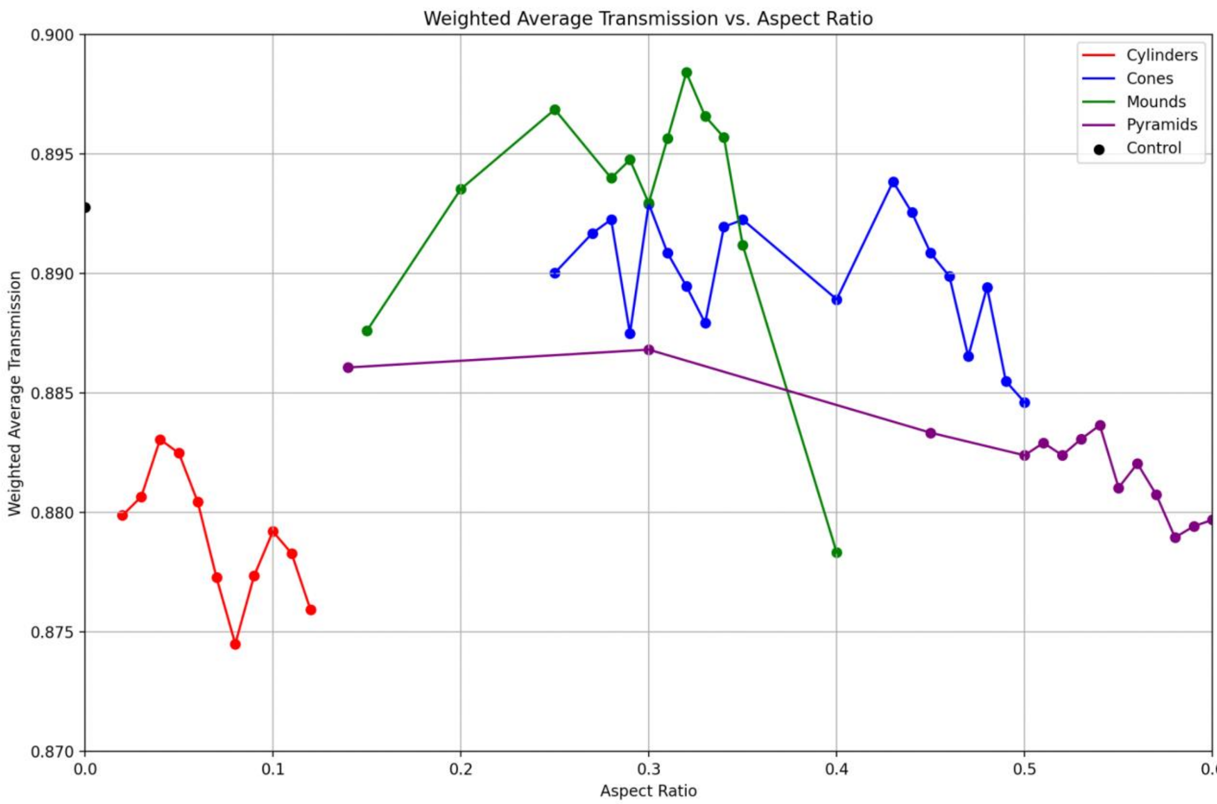

Figure 9: The graph plots the calculated weighted averages for the transmission of the aspect ratios in the optimal range for each geometry. Please note that the axes are truncated to highlight trends.

As shown in Figure 9, considering varying solar insolation at differing incident angles, the most optimal geometry was a mound-shaped geometric ARC with a height-to-diameter ratio of 0.32, which produced a weighted average light transmission of 0.8984. This performance can be attributed to its high light transmittance at large incident angles and its reasonable, albeit not the greatest, light transmittance at small incident angles. Shockingly, both the cylinder and pyramid geometries failed to register a weighted average light transmission that outperformed the flat control group, which recorded a weighted average light transmission of 0.8928.

It is important to note that for any individual shape, the transmission is accurate for any equivalent aspect ratio of differing dimensions, assuming 0 parasitic absorbance. When larger dimensions are used, parasitic absorption must be considered, and the transmission would decrease. This effect exacerbates the performance of larger height structures, meaning the solar cell would absorb even less than what the low transmission proportions shown by the simulations already indicate for larger aspect ratios. Thus, when implementing these geometric ARCs, it is ideal to fabricate the structures with the appropriate aspect ratios to the smallest possible scale to mitigate the impact of parasitic absorption.

As to the material, disadvantages of SiO_2 include difficulty in implementation on large-scale areas and the need for additional thermal treatments when utilizing sol-gel mechanisms for fabrication [9]. This can be avoided by utilizing another approach, such as some sort of imprint lithography, to improve scaling capabilities. During and after production, numerous processing methods can be utilized to enhance SiO_2's light transmission and reduce its glare [9]. There are a multitude of potential manufacturing processes for these textures, including various types of sol-gel mechanisms and imprint lithographies [9], [19].

Conclusion

Ultimately, this study highlights the value of optimizing geometric ARCs' shape and dimensions in order to increase the light absorption of a solar cell by displaying results that solar panel manufacturers and researchers can utilize. Immediately, with these results, modifications to existing solar panels to match the shape and dimension that worked best across different incident light angles can be made to expand electricity generation capabilities based on the main takeaway that the optimized geometric ARC shape differs for varying angles of incidence. For solar panels with dual-axis tracking capabilities, the surface of the solar panel remains facing the sunlight, meaning light rays approach the solar panel at an incident angle of 0°. The pyramid ARC texture with a height-to-side ratio of 0.52 would maximize light absorption for such solar panels, increasing light transmission by 0.71%. On the other hand, for fixed solar panels, the mound ARC texture with an aspect ratio of 0.32 would be best suited to maximizing light absorption, increasing light transmission by roughly 0.63%.

Avenues for further research include algorithmically optimizing the parameters of the dimensions of the shapes to determine the most efficient geometric ARC. Furthermore, more shapes and patterns are needed, including texturizing more layers and texturizing the underside of the glass. For example, adding more structures within the gaps between the shapes could be a potential pattern to examine. Random texturizations must be considered too. Also, embedding ARC textures along the encapsulant ethylene-vinyl acetate (EVA) layer on top of the solar cell is a potential option, and implementing printing methods with a polymer substance would be uncomplicated. Using more oval-like shapes should be tested as well, as the base of the mound patterns in this simulation was not modified, remaining circular. Another idea is to modify the curvature of the mound shape itself. Increasing the gaps between the structures could be potentially explored, yet it is not recommended, as previous studies have found that increasing the texturization period reduces the anti-reflection effect [20]. Finally, modifying the ways in which the light rays approach the structures to more accurately resemble the changing direction of sunlight throughout the day with a more elaborate optimization process would improve the practicality and applicability of the simulation.

In general, reducing losses due to light reflection would increase power output, making monumental progress in helping abate fossil fuel dependency and strengthening the environment. Furthermore, as the globe struggles to transition to renewable energy sources, constructing a more optimal solar panel would draw the public and corporations to adopt solar power, diverting focus from non-renewable energy sources.

Code and Data Availability

Here is the link to the GitHub repository used for the simulations, along with the data: https://github.com/aj24by7/pvtrace-aj

Acknowledgements

This research project was mentored by PhD student Shomik Verma, who offered expertise through the research process as well as contributed to the code. Also, revisions and formatting advice were given by Ramesh Munamarty.

References

[1] N. Shanmugam, R. Pugazhendhi, R. Madurai Elavarasan, P. Kasiviswanathan, and N. Das, “Anti-Reflective Coating Materials: A Holistic Review from PV Perspective,” Energies, vol. 13, no. 10, p. 2631, May 2020, doi: 10.3390/en13102631.
[2] J. Escarré et al., “Geometric light trapping for high efficiency thin film silicon solar cells,” Sol. Energy Mater. Sol. Cells, vol. 98, pp. 185–190, Mar. 2012, doi: 10.1016/j.solmat.2011.10.031.
[3] C. Ji et al., “Recent Applications of Antireflection Coatings in Solar Cells,” Photonics, vol. 9, no. 12, p. 906, Nov. 2022, doi: 10.3390/photonics9120906.
[4] A. Peter Amalathas and M. Alkaisi, “Nanostructures for Light Trapping in Thin Film Solar Cells,” Micromachines, vol. 10, no. 9, p. 619, Sep. 2019, doi: 10.3390/mi10090619.
[5] S. Bong et al., “Effective Light Trapping in Thin Film Silicon Solar Cells with Nano- and Microscale Structures on Glass Substrate.,” J. Nanosci. Nanotechnol., vol. 16, no. 5, pp. 4978–4983, May 2016, doi: 10.1166/jnn.2016.12179.
[6] A. M. Law, L. O. Jones, and J. M. Walls, “The performance and durability of Anti-reflection coatings for solar module cover glass – a review,” Sol. Energy, vol. 261, pp. 85–95, Sep. 2023, doi: 10.1016/j.solener.2023.06.009.
[7] B. G. Priyadarshini and A. K. Sharma, “Design of multi-layer anti-reflection coating for terrestrial solar panel glass,” Bull. Mater. Sci., vol. 39, no. 3, pp. 683–689, Jun. 2016, doi: 10.1007/s12034-016-1195-x.
[8] A. Deinega, I. Valuev, B. Potapkin, and Y. Lozovik, “Minimizing light reflection from dielectric textured surfaces,” J. Opt. Soc. Am. A, vol. 28, no. 5, p. 770, May 2011, doi: 10.1364/JOSAA.28.000770.
[9] Z. Han, Z. Jiao, S. Niu, and L. Ren, “Ascendant bioinspired antireflective materials: Opportunities and challenges coexist,” Prog. Mater. Sci., vol. 103, pp. 1–68, Jun. 2019, doi: 10.1016/j.pmatsci.2019.01.004.
[10]danieljfarrell, “pvtrace/pvtrace at master · danieljfarrell/pvtrace,” GitHub. Accessed: Jul. 11, 2025. [Online]. Available: https://github.com/danieljfarrell/pvtrace/tree/master/pvtrace
[11]S. Verma, shomikverma/pvtrace-sv. (Jan. 30, 2025). Python. Accessed: Jul. 11, 2025. [Online]. Available: https://github.com/shomikverma/pvtrace-sv
[12]S. Verma, D. J. Farrell, and R. C. Evans, “Ray-Trace Modeling to Characterize Efficiency of Unconventional Luminescent Solar Concentrator Geometries,” ACS Appl. Opt. Mater., vol. 1, no. 5, pp. 1012–1025, May 2023, doi: 10.1021/acsaom.3c00074.
[13]“Fused Silica SiO2 Optical Material | Crystran.” Accessed: Jul. 11, 2025. [Online]. Available: https://www.crystran.com/optical-materials/fused-silica-sio2
[14]W. D. Putri and G. W.P. Adhyaksa, “Nano Pyramid Anti–reflective Coating Design for Improved Thin-Silicon Photovoltaics,” in Proceedings of the International Conference on Sustainable Engineering, Infrastructure and Development, ICO-SEID 2022, 23-24 November 2022, Jakarta, Indonesia, Jakarta, Indonesia: EAI, 2023. doi: 10.4108/eai.23-11-2022.2339154.
[15]I. H. Malitson, “Interspecimen Comparison of the Refractive Index of Fused Silica*,†,” JOSA Vol 55 Issue 10 Pp 1205-1209, Oct. 1965, doi:

10.1364/JOSA.55.001205.
[16]A. A. Fashina, M. G. Zebaze Kana, and W. O. Soboyejo, “Optical reflectance of alkali-textured silicon wafers with pyramidal facets: 2D analytical model,” J. Mater. Res., vol. 30, no. 7, pp. 904–913, Apr. 2015, doi: 10.1557/jmr.2015.70.
[17]Y. Li, M.-Y. Lee, H.-W. Cheng, and Z.-L. Lu, “3D simulation of morphological effect on reflectance of Si3N4 sub-wavelength structures for silicon solar cells,” Nanoscale Res. Lett., vol. 7, no. 1, p. 196, Dec. 2012, doi: 10.1186/1556-276X-7-196.
[18]“Solar Time, Angles, and Irradiance Calculator - User Manual | New Mexico State University - BE BOLD. Shape the Future.” Accessed: Jul. 10, 2025. [Online]. Available: https://pubs.nmsu.edu/_circulars/CR674/index.html
[19]M. Modaresialam, Z. Chehadi, T. Bottein, M. Abbarchi, and D. Grosso, “Nanoimprint Lithography Processing of Inorganic-Based Materials,” Chem. Mater., vol. 33, no. 14, pp. 5464–5482, Jul. 2021, doi: 10.1021/acs.chemmater.1c00693.
[20]Y. F. Makableh, M. Al-Fandi, M. Khasawneh, and C. J. Tavares, “Comprehensive design analysis of ZnO anti-reflection nanostructures for Si solar cells,” Superlattices Microstruct., vol. 124, pp. 1–9, Dec. 2018, doi: 10.1016/j.spmi.2018.10.003.